Check for updates

MR-Guided Radiotherapy for Brain and Spine Tumors

Danilo Maziero[1], Michael W. Straza[2], John C. Ford[1], Joseph A. Bovi[2], Tejan Diwanji[1], Radka Stoyanova[1], Eric S. Paulson[2] and Eric A. Mellon[1]*

[1] Department of Radiation Oncology, Sylvester Comprehensive Cancer Center, Miller School of Medicine, University of Miami, Miami, FL, United States, [2] Department of Radiation Oncology, Medical College of Wisconsin, Milwaukee, WI, United States

MRI is the standard modality to assess anatomy and response to treatment in brain and spine tumors given its superb anatomic soft tissue contrast (e.g., T1 and T2) and numerous additional intrinsic contrast mechanisms that can be used to investigate physiology (e.g., diffusion, perfusion, spectroscopy). As such, hybrid MRI and radiotherapy (RT) devices hold unique promise for Magnetic Resonance guided Radiation Therapy (MRgRT). In the brain, MRgRT provides daily visualizations of evolving tumors that are not seen with cone beam CT guidance and cannot be fully characterized with occasional standalone MRI scans. Significant evolving anatomic changes during radiotherapy can be observed in patients with glioblastoma during the 6-week fractionated MRIgRT course. In this review, a case of rapidly changing symptomatic tumor is demonstrated for possible therapy adaptation. For stereotactic body RT of the spine, MRgRT acquires clear isotropic images of tumor in relation to spinal cord, cerebral spinal fluid, and nearby moving organs at risk such as bowel. This visualization allows for setup reassurance and the possibility of adaptive radiotherapy based on anatomy in difficult cases. A review of the literature for MR relaxometry, diffusion, perfusion, and spectroscopy during RT is also presented. These techniques are known to correlate with physiologic changes in the tumor such as cellularity, necrosis, and metabolism, and serve as early biomarkers of chemotherapy and RT response correlating with patient survival. While physiologic tumor investigations during RT have been limited by the feasibility and cost of obtaining frequent standalone MRIs, MRIgRT systems have enabled daily and widespread physiologic measurements. We demonstrate an example case of a poorly responding tumor on the 0.35 T MRIgRT system with relaxometry and diffusion measured several times per week. Future studies must elucidate which changes in MR-based physiologic metrics and at which timepoints best predict patient outcomes. This will lead to early treatment intensification for tumors identified to have the worst physiologic responses during RT in efforts to improve glioblastoma survival.

Keywords: glioblastoma, brain and spine tumors, MRI, MRgRT, radiotherapy, pseudoprogression

INTRODUCTION

Despite the potential of Magnetic Resonance image guided Radiation Therapy (MRgRT) to treat brain tumors, a recent review (1) highlighted that only one out of twenty recent studies used MRgRT to treat brain tumor patients (2). This is because MRgRT has been almost exclusively applied to treat moving tumors located in the torso, such as in the lungs (3), breast (4), pancreas (5, 6), liver (7), prostate (8) and pelvis (9). Tumor and healthy tissue in these regions can move significantly between or during treatments due to physiological motion such as respiration (3, 10, 11), digestion (12), and involuntary movements (13). Additionally, target geometry may change during treatment from tumor growth or shrinkage or patient weight loss or gain. Therefore, MRgRT has been applied to detect and compensate motion, as well as detect and compensate for daily anatomic changes with rapid radiotherapy (RT) plan updates. These implementations of MRgRT are commonly termed "adaptive radiotherapy" and are available within existing MRgRT products. Since this existing workflow adapts to anatomy, we propose that these techniques be termed "anatomic adaptive radiotherapy."

MRI can also provide physiologic information such as tumor cellularity, vascularity, and metabolism that correlate with radiotherapy response. For example, changes in regional water mobility are detectable by diffusion weighted imaging (DWI) and are associated with increased cellularity (tumor growth) or necrosis (14, 15). Increased blood volume and flux (16) can be estimated from perfusion MRI and correlate to tumor oxygen consumption (16). Tumor extension and aggressiveness are also associated with its metabolic profile and can be estimated by magnetic resonance spectroscopy (17) (MRS). Among others, these techniques are collectively termed multiparametric MRI (mpMRI). Since changes in mpMRI during RT correlate with eventual tumor response (18–20), there is significant interest within the MRgRT community in adapting RT to mpMRI findings (21). For example, if mpMRI demonstrates that a tumor is increasingly cellular, metabolic, and angiogenic during treatment (i.e., resistant to standard therapies), should RT dose-escalation or other additional therapies be considered? When adapting RT to changes in tumor physiology, these applications can be called "physiologic adaptive radiotherapy" (PART).

Studies of physiologic changes during fractionated RT are not currently widespread because it has never been feasible before MRgRT systems to obtain mpMRI on a daily basis. It has been very difficult to obtain image data weekly due to the cost and logistics of scanning RT patients every week on diagnostic MRI scanners. Therefore, existing data of mpMRI during RT has been limited to a small number of institutions and patients and a limited number of time points (typically once or twice during a 6-week course of RT). While this data has been promising, MRgRT devices allow the possibility of obtaining mpMRI with high frequency throughout treatment to elucidate trends in tumor physiology that can be leveraged to make adaptive treatment decisions. With this in mind, this review discusses the potential use of anatomic and physiologic adaptive radiotherapy for treating brain and spine tumors with an emphasis on glioblastoma.
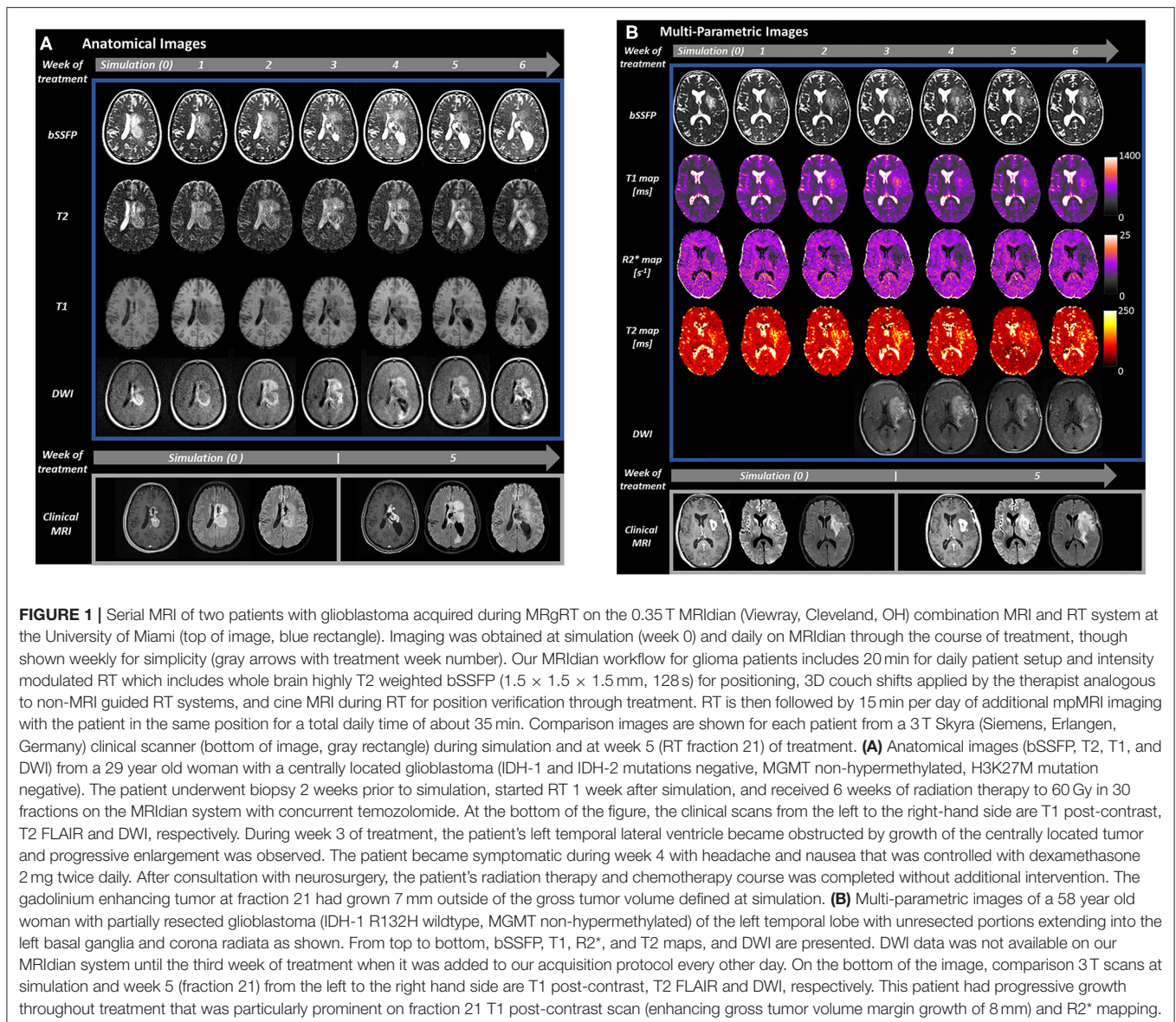
ADAPTIVE RADIOTHERAPY FOR BRAIN TUMORS

Intrafraction motion is typically not a major concern for brain tumors given the use of thermoplastic masks to immobilize the patient's head and negligible physiologic motion. However, interfraction changes in tumor size can be problematic in numerous scenarios. For example, certain tumors can have rapid cyst expansion, which has been most commonly described for craniopharyngioma (22). This leads to a recommendation for weekly or bi-weekly diagnostic MRI to ensure appropriate target dose coverage and adapt RT plans offline to anatomic changes if needed. While it has not yet been reported in the literature, cysts can be monitored on an MRgRT system and RT can be adapted easily without requiring standalone diagnostic MRIs. Additionally, edema and resection cavities are visualized with default imaging on the initial version of the 0.35T MRI system (2). For example, at University of Miami during a course of conventionally fractionated RT we have used scans obtained with MRgRT to identify or rule out serious pathologies in patients with headaches during treatment, identify edema increase or decrease during RT, and reassure patients, manage steroid doses, or consult neurosurgery based on findings (e.g., **Figure 1A**).

Glioblastoma

Glioblastoma is the most common cancer originating in the brain with ~12,000 new diagnoses per year in the U.S.A. and median survival about 18 months (23–25). First-line treatment for glioblastoma includes biopsy or resection followed by 6 weeks of RT with concurrent temozolomide chemotherapy and 6–12 months of continued temozolomide (26). Clinically, MRI is obtained before RT for planning and then 1 month after RT to assess early response, usually an interval of ~3 months.

Anatomic Changes in Glioblastoma During RT

T1 post-contrast and T2-FLAIR images are typically used for determining tumor response to treatment, most commonly by applying criteria specified by Response Assessment in Neuro-Oncology (RANO) (27). Up to 49% of patients with glioblastoma demonstrate growth on T1 gadolinium-enhanced MRI acquired after the 6 weeks of standard chemoradiation treatment (28, 29). Patients with true progression of non-responding tumor continue to progress on serial MRIs and often die within 9 months (30–32). Some patients with growth on MRI after chemoradiation will stabilize or spontaneously regress without treatment modification, a condition termed pseudoprogression (30–32). This condition reflects therapy response with recruitment of blood vessels and/or necrosis and improved median survival ~38 months (28, 33). Unfortunately, no current technique reliably distinguishes true progression and pseudoprogression when these changes are present within the

FIGURE 1 | Serial MRI of two patients with glioblastoma acquired during MRgRT on the 0.35 T MRIdian (Viewray, Cleveland, OH) combination MRI and RT system at the University of Miami (top of image, blue rectangle). Imaging was obtained at simulation (week 0) and daily on MRIdian through the course of treatment, though shown weekly for simplicity (gray arrows with treatment week number). Our MRIdian workflow for glioma patients includes 20 min for daily patient setup and intensity modulated RT which includes whole brain highly T2 weighted bSSFP (1.5 × 1.5 × 1.5 mm, 128 s) for positioning, 3D couch shifts applied by the therapist analogous to non-MRI guided RT systems, and cine MRI during RT for position verification through treatment. RT is then followed by 15 min per day of additional mpMRI imaging with the patient in the same position for a total daily time of about 35 min. Comparison images are shown for each patient from a 3 T Skyra (Siemens, Erlangen, Germany) clinical scanner (bottom of image, gray rectangle) during simulation and at week 5 (RT fraction 21) of treatment. **(A)** Anatomical images (bSSFP, T2, T1, and DWI) from a 29 year old woman with a centrally located glioblastoma (IDH-1 and IDH-2 mutations negative, MGMT non-hypermethylated, H3K27M mutation negative). The patient underwent biopsy 2 weeks prior to simulation, started RT 1 week after simulation, and received 6 weeks of radiation therapy to 60 Gy in 30 fractions on the MRIdian system with concurrent temozolomide. At the bottom of the figure, the clinical scans from the left to the right-hand side are T1 post-contrast, T2 FLAIR and DWI, respectively. During week 3 of treatment, the patient's left temporal lateral ventricle became obstructed by growth of the centrally located tumor and progressive enlargement was observed. The patient became symptomatic during week 4 with headache and nausea that was controlled with dexamethasone 2 mg twice daily. After consultation with neurosurgery, the patient's radiation therapy and chemotherapy course was completed without additional intervention. The gadolinium enhancing tumor at fraction 21 had grown 7 mm outside of the gross tumor volume defined at simulation. **(B)** Multi-parametric images of a 58 year old woman with partially resected glioblastoma (IDH-1 R132H wildtype, MGMT non-hypermethylated) of the left temporal lobe with unresected portions extending into the left basal ganglia and corona radiata as shown. From top to bottom, bSSFP, T1, R2*, and T2 maps, and DWI are presented. DWI data was not available on our MRIdian system until the third week of treatment when it was added to our acquisition protocol every other day. On the bottom of the image, comparison 3 T scans at simulation and week 5 (fraction 21) from the left to the right hand side are T1 post-contrast, T2 FLAIR and DWI, respectively. This patient had progressive growth throughout treatment that was particularly prominent on fraction 21 T1 post-contrast scan (enhancing gross tumor volume margin growth of 8 mm) and R2* mapping.

radiotherapy field. Therefore, RANO criteria suggest follow-up imaging over the next 3–6 months to assess whether changes spontaneously resolve without modification of therapy or continue to progress.

Consistent with these well-known changes, a recent series of 14 patients treated with MRgRT identified T2-weighted volume increases >25% in 4 patients who had been scanned daily during RT treatment delivery (34). Most growth occurred late in treatment for three of the four patients, a previously unreported finding that could hold prognostic significance. Another study observed meaningful tumor dynamic changes during chemoradiation therapy by analyzing T1 post-contrast and T2-Flair images of 62 patients with glioblastoma (35). Since the amount of gadolinium enhancement is the primary metric used currently to evaluate glioblastoma evolution, a challenge to the MRgRT community in evaluating glioblastoma changes

during RT is when and how often to administer gadolinium contrast during RT; or whether to use alternative measures of tumor growth. While it is unclear whether frequent gadolinium poses risks to non-allergic subjects with normally functioning kidneys, there is significant concern about potential gadolinium deposition in the brain due to repeated administrations and unclear symptoms that may associate with gadolinium (36).

Multiparametric MRI of Glioblastoma for Response Assessment

Existing data suggests that there is an evolution in tumor physiologic changes that occur in glioblastomas during RT. Different MRI contrasts such as T1-weighted (37), T2-weighted (38), Perfusion (39), Diffusion Weighted Imaging (DWI) (40) and proton Magnetic Resonance Spectroscopy (MRS) (41) have been investigated for early detection of glioblastoma response to

treatment. Many of these techniques have been implemented or are in development on MRgRT devices, and an example is given in **Figure 1B**.

T1 and T2 and Quantitative Multi-Parametric Mapping MRI

Spin-lattice (T1) and spin-spin (T2) relaxations are mechanisms intrinsic to the tissues and measurable by MRI. The different rates of relaxation can be mapped, and quantitative measures of MRI changes can be provided. For example, quantitative multi-parametric mapping (qMPM) is a technique to obtain multiple MRI parameters in a short amount of time (42). This technique has allowed for fast and accurate mapping of different relaxation parameters such as R1 (1/T1), R2* (1/T2*), and R2 (1/T2) and their association with glioblastoma diagnosis. A previous study showed that R1 and R2 maps identify shorter relaxation times for voxels closer than further from the tumor, which was suggested to reflect tumor invasion (43). Other studies have shown promising results for using qMPM to detect sites of future tumor progression (44) and to early detect tumor progression in patients undergoing treatment with bevacizumab (45).

There may be some benefit of these quantitative measures in assessing glioblastoma response. A recent study showed the feasibility of applying the Strategically Acquired Gradient Echo (STAGE) (46) to obtain R1, R2*, and Proton Density (PD) maps in patients with GBM after each fraction by using the 0.35T MRI-linac system (47). Another study used MR fingerprinting to obtain these maps using the 1.5T MRI-linac system (48). The capability of observing tumor response to treatment via its size and relaxation time variations over the course of fractionated RT is an important step toward using MRgRT to adapt glioblastoma radiation treatment.

Perfusion

There are two main methods for measuring perfusion with gadolinium using MRI: Dynamic Susceptibility Contrast (49) (DSC) and Dynamic Contrast Enhancement (50) (DCE). DSC is based on detecting T2* signal loss due to susceptibility effects from the passage of a bolus of gadolinium contrast agent (51). This method is used for estimating hemodynamic related parameters of relative cerebral blood flow (rCBF) and relative cerebral blood volume (rCBV) (52, 53), which are reported as the most sensitive parameters for differentiating tumor progression from pseudoprogression after RT (54). Multiple post-RT studies have shown that tumor progression is associated with higher values of rCBV in comparison to pseudoprogression (19, 55, 56). Alternatively, DCE parameters are obtained by detecting signal increases from dynamic acquisition of T1-weighted images during a gadolinium bolus passage (57). The resultant signal changes are used to estimate parameters such as area under the curve (AUC) and volumetric transfer constant (K^{trans}), fractional blood plasma volume (Vp) and extracellular volume (Ve) (58). The K^{trans} and AUC are the DCE-derived parameters consistently reported to be higher for recurrent gliomas when compared to radiation necrosis and pseudoprogression (59–61).

MRI perfusion derived parameters have been shown to change due to chemoradiation treatment and correlate with eventual patient outcome (62, 63). For example, CBF and K^{trans} increased 30 and 10%, respectively, when DSC and DCE data from 2 weeks after treatment completion were compared to pre-treatment data (16). Larger increases were associated with shorter patient survival when compared to patients showing smaller CBF and K^{trans} changes (16). In another study, reduction in CBV post-treatment was associated with doubling of patient survival compared with patients showing increased CBV (19). Other DCE-based parameters have also been shown to change significantly due to treatment. For example, a larger decrease on volumetric plasma volume 90th percentile histogram (VP$_{90\%}$) of DCE data acquired before and after treatment was associated with pseudoprogression when compared to true progression (-39.6 vs. -2.6%) (60). Changes in perfusion parameters have also been reported for data acquired during chemoradiation treatment. For example, patients showing tumor progression presented a significantly reduced rCBV during week three of treatment when compared to pseudoprogression patients (64). Another study acquired perfusion data weekly during chemoradiotherapy to evaluate tumor perfusion response to antiangiogenic therapy during a clinical trial (65). The MRI-linac systems can provide frequent data for evaluating perfusion parameters more frequently over the course of radiotherapy. Alternatives to gadolinium such as arterial spin labeling (ASL) (66) and intra-voxel incoherent motion (IVIM) (67) may be promising to evaluate survival of patients with gliomas (68, 69) and even daily measurements during RT to evaluate tumor response may be possible on MRI-linac systems without the added risk of exogenous contrast.

Diffusion

Diffusion weighted imaging (DWI) is an MRI modality capable of measuring the apparent diffusion coefficient (67) (ADC), an estimate of Brownian motion of water molecules within an imaging voxel. Water molecules in the intra-cellular environment experience a highly restricted environment, while water molecules present in the extra-cellular environment experience relatively unrestricted diffusion (70). Thus, low ADC correlates with areas of high tumor cellularity (71, 72) and aggressiveness (14, 73).

Changes in tumor ADC during post-treatment follow up images is also capable of differentiating true progression from pseudoprogression and radiation necrosis (15, 74). The rationale is that while tumor growth increases cellular density and decreases regional water mobility, a successful treatment causes the breakdown of cellular membranes of the tumor, decreases regional cellular density, and increases water mobility (18, 75). For example, Elson and colleagues reported the potential use of ADC as an early marker for responsiveness to treatment of glioblastoma. The authors analyzed ADC values from voxels within the T2/Flair volume from 52 patients and verified that elevated minimum and mean ADC values are significantly correlated to Progression Free Survival (PFS) and Overall Survival (OS) (75). Additional metrics derived from DWI such as fraction, linear, planar and spherical anisotropy have also been reported to distinguish true progression from pseudoprogression (74).

The observation of ADC over time is the base for functional Diffusion Mapping (fDM) (76), a biomarker discussed as an early detector of tumor response to treatment and survival rate (14, 77–79). For example, a previous study analyzed DWI data from 60 patients undergoing concomitant RT and temozolomide (18). The authors generated fDM maps using data acquired before, 3 and 10 weeks after the start of treatment. In their results, they showed that patients with increasing number of high ADC value voxels during treatment have a longer survival rate when compared to patients with increasing number of low ADC voxels (52.6 vs 10.9 months). The fDM technique depends on several variables related to the ADC maps generation and evaluation, such as the metric chosen and thresholding for classifying voxels showing significantly increased, decreased, or stable ADC values over time. Although previous studies showed that all of these concerns can be overcome (80), the choice and number of measurement points has still been challenging, among other reasons due to scanning time availability and patient tolerance of standalone MRIs. A practical benefit of daily MRgRT is daily mpMRI to identify the best time points for comparisons or identify trends as well as consistent scanner parameters across centers.

A longitudinal evaluation of ADC maps obtained during fractionated therapy of head and neck tumors was demonstrated by Yang et al. using the 0.35T MRI-linac system (81). The group showed that the ADC values from a ROI within responding tumor increased consistently during treatment, while the ADC values from a volume not treated (brain stem) stayed the same. We believe that further studies should be done to evaluate the feasibility of obtaining more complex DWI-based maps such as fDM and fractional anisotropy using the MRI-linac systems to show tumor early response to treatment and allow for early planning adaptation.

Spectroscopy

Proton magnetic resonance spectroscopy (MRS) is a non-invasive method capable of estimating the concentration of different tumor-related metabolites in the brain (82). High ratios of Choline (Cho)/N-acetyl-aspartate (NAA), Cho/normalized Creatine (nCR), Cho/normalized Choline (nCho) are known to correlate with tumor grade (83). Specifically, Cho correlates to Ki-67 index, which reflects tumor proliferation of gliomas (84, 85). A high ratio (Cho)/(NAA) has been reported as a biomarker of tumor presence and is useful for delimitating glioma extension and infiltration using MRS (17, 86, 87) and MR spectroscopic imaging (MRSI) (88, 89). Given the known correlations of MRS with tumor aggressiveness and cellularity, MRSI has been integrated into the RT planning workflow in one study to select areas for dose escalation (90). Other metrics such as the choline-to-NAA index (CNI) are also commonly investigated as potential predictors of patient outcome (41).

MRS has also been applied to detect changes of metabolites during radiotherapy treatment and to associate them with patient outcome. A previous study reported that patients showing large decreases of normalized Cho from the fourth week of treatment to 2 months post-treatment correlated with a worse median OS and PFS than patients not showing such decreases (91).

Another study compared MRS data from pre-RT to data from the third week of treatment and showed that patients with stable or decreased median or mean Cho/NAA ratio showed less risk of tumor progression than patients presenting increased Cho/NAA ratios over the same period (20).

We believe that the implementation of MRS sequences is technically viable on MRI-linac devices to measure metabolism during therapy. However, to the best of our knowledge it has not been done. Such implementation would allow for a more frequent evaluation of metabolites throughout chemoradiation treatment to associate early glioblastoma response to treatment. For example, glutamate and glutamine (Glx) metabolism is altered in glioblastoma, and detection of Glx is facilitated at low field (92). Glx detected by single voxel spectroscopy at 0.5T had 2-fold increase of signal-to-noise compared to 1.5T in the brains of healthy volunteers due to collapse of the C3 and C4 Glx J-coupled resonances into a "pseudo-singlet" 2.35 ppm peak at 0.5T (93). Such implementations at 0.35 T would likely be with low resolution single voxel spectroscopy that could give additional information about pseudoprogression or true progression for PART. Conversely, on 3 T scanners, whole brain Cho/NAA ratio MRSI with $5.6 \times 5.6 \times 10$ mm resolution acquired in 15 min has been integrated into RT planning and response tracking workflows that could be considered for adaptive RT (94, 95). MRSI could theoretically be acquired on a 1.5 T MRgRT system as well, though it is unclear whether Cho/NAA MRSI on a 1.5 T MRgRT system might have suitable resolution and spectral quality for adaptive RT.

Combining Different Contrasts and Modeling Radiomics

In the sections above we described results of studies associating individual MRI contrast findings to glioblastoma detection and tumor response to treatment. However, several studies showed evidence that combining different contrasts and extracting multiple parameters from MRI improves the sensitivity of predicting patient outcomes (41, 72–74). Combining radiomics metrics from multiparametric MRI to clinical variables is also an important tool for predicting tumor treatment outcome (96). This approach has also been showed to benefit from the availability of multiparametric MRI. For example, the combination of multiparametric MRI for radiomics modeling was shown to predict patient overall survival using data from before chemoradiation therapy (97). Another, study showed that combining diffusion and perfusion weighted MRI for radiomics modeling improves prediction performance when compared to a model based only on conventional MRI or clinical predictors (98). The availability of MRI data from every radiotherapy fraction allows for the inclusion of a high sampling rate temporal component into radiomics modeling.

Technical Challenges and Limitations

Another challenge for obtaining high quality images with MR-Linac systems is related to the relatively decreased signal to noise ratio when compared to images from higher magnetic fields ($\geq$1.5T). Therefore, a compromise among temporal and spatial resolutions is inevitable. However, strong efforts are being
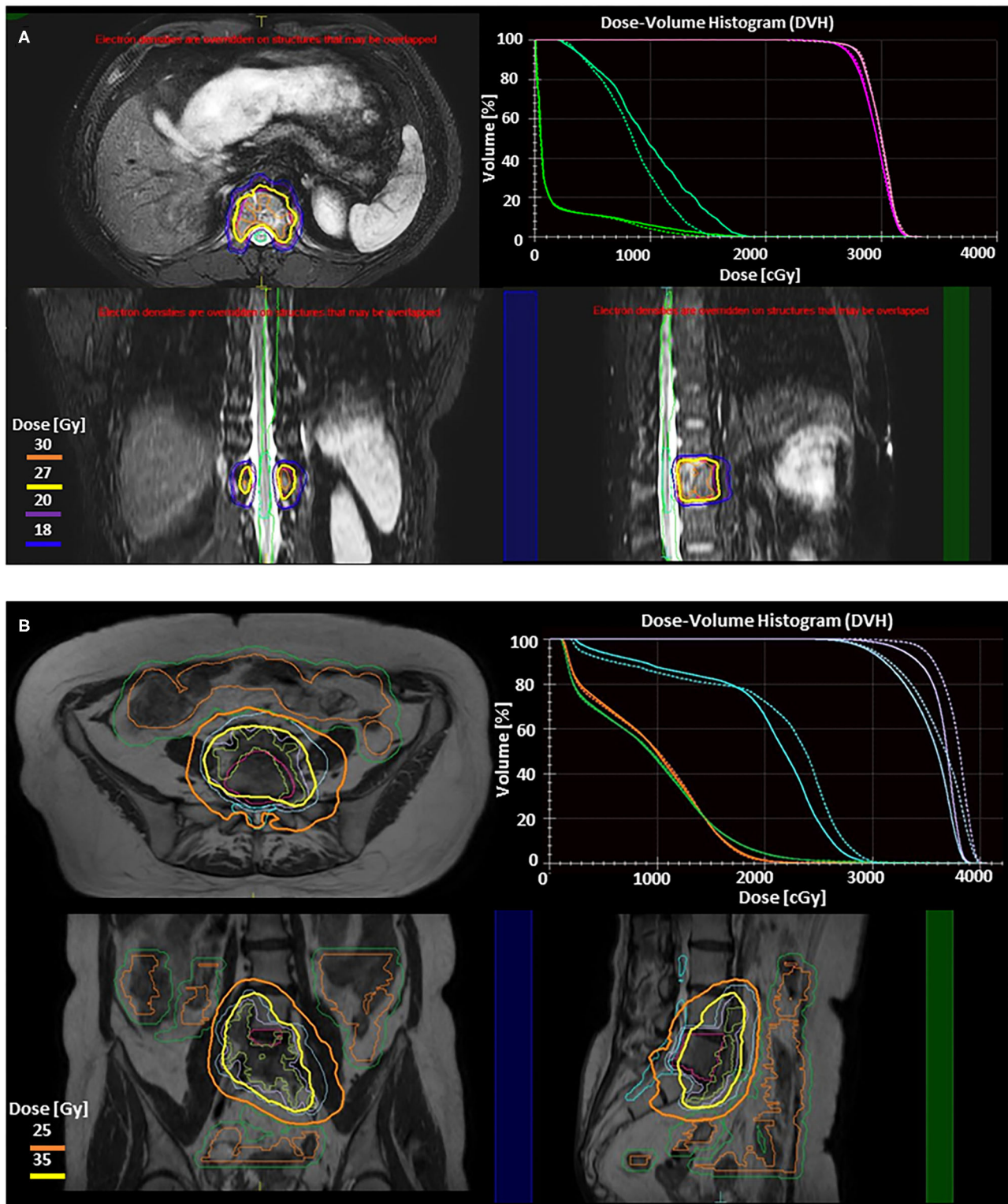
FIGURE 2 | Illustration of two adaptive approaches on the 1.5 T Elekta Unity (Stockholm, Sweden) MRgRT system for stereotactic body radiotherapy (SBRT) of spine metastases. Adapt to position (ATP) is used to correct for translational shifts by adjusting beam apertures and weights without altering reference contours. Adapt to shape (ATS) accounts for all interfraction changes by re-optimizing the plan based on the MRI of the day, and requires adjustment of the target and adjacent organ at risk (OAR) contours. These treatment strategies have been described elsewhere as well as their utilization for upper abdominal SBRT (109, 110). Real-time cine MRIs

(Continued)

FIGURE 2 | acquired in perpendicular planes through the PTV center of mass are used to monitor the target during radiation delivery. **(A)** Axial, sagittal, and coronal slices from 3D T2 fat suppressed MR images from Unity showing ATP SBRT plan to T12 metastatic thyroid lesion (GTV Pink, PTV Magenta). Prescription was 27 Gy (yellow) in 3 fractions. 30 Gy (orange), 20 Gy (purple), and 18 Gy (blue) isodose lines are also shown. DVH in right upper panel compares the reference plan (solid lines) to the adaptive plan (dashed lines). This case involves a thoracic vertebrae metastasis without any extraosseous component. The target had good separation from dose limiting organs at risk without large variations in either target or OAR position or shape, making an ATP adaptive workflow optimal as recontouring is not necessary. For ATP, after the patient is positioned on the table daily MR images are obtained, fused with the reference plan, and shifts reviewed and approved by physician prior to beginning adaptation. During the adaptive process, mpMRI can be obtained simultaneously. Once a new plan is calculated, it can be reviewed by the physician, along with a verification MR and real-time cine MRI to confirm no significant intrafraction motion. The dose volume histogram (DVH) in the right upper panel demonstrates preserved target coverage with improved OAR doses for treatment. For conventionally fractionated treatments, total time on the table for patients range from 18 to 26 min, while this patient's SBRT delivery ranged from 40 to 60 min per treatment. **(B)** Axial, coronal, and sagittal slices from T2 MR images from Unity showing ATS fraction of SBRT plan to colorectal metastasis at L5 with anterior extraosseous extension. Prechemotherapy volume (blue) was prescribed 25 Gy in 5 fractions (orange) while Post-chemotherapy volume (purple) was prescribed 35 Gy in 5 fractions (yellow). DVH in right upper panel compares reference plan (solid lines) to the adaptive plan (dashed lines), demonstrating isotoxic treatment to the cauda (teal), small bowel (orange), and small bowel PRV (green) while improving coverage to both target volumes. Here the target is within close proximity to both large and small bowel. Here we use the ATS approach, with a unique parallel contouring work flow that has been described elsewhere (111). The target was rigidly fused on the daily MR, but bowel contours were different for each of five daily fractions, requiring recontouring. This allowed for maintenance of target coverage without violation of OAR constraints. ATS workflows take longer due to time required for recontouring and adapting the reference plan to not just translational shifts but new relative anatomy. For this patient the total table time ranged from 59 to 70 min.

applied toward developing and improving data acquisition and reconstruction strategies, such as parallel imaging and non-cartesian k-space trajectories (99). Such strategies provide for fast k-space data sampling and allow more averages of the object being imaged, resulting in higher SNR images than those obtained from standard approaches. Additionally, model-based reconstruction frameworks, such as motion-corrected and high-resolution anatomically assisted (100) and image quality transfer (101) also have been shown as alternatives for improving spatial resolution of low-resolution images.

Finally, MRgRT allows for MRI acquisition while dose is delivered, which may allow for the observation of tumor changes within a single RT fraction. For example, MRI thermometry could be used to verify tumor heating during RT with hyperthermia (102) or blood oxygen level dependent MRI could monitor the increased blood flow to tumors that occurs with carbogen inhalation (103). Such approaches may be challenging, as temporal signal variances detected during radiation delivery can be related to magnetic field drifts and susceptibility artifacts due to multi-leaf-collimator movements (104).

STEREOTACTIC RADIOTHERAPY OF BRAIN AND SPINE METASTASES

The anatomic and physiologic adaptive radiotherapy discussed above might also be applied to short courses of radiotherapy (1–5 fraction over up to 2 weeks) commonly used in brain and spine metastases (105). In resected brain metastases, significant volume changes can happen if radiotherapy must start soon after resection (106). For example, one study showed that 9 out of 22 patients required treatment adjustments based on repeat MRI within 7 days after planning MRI and 7 out of 9 patients required adjustments in between 8 and 14 days after planning MRI (107). This suggests that anatomic adaptation might be helpful for longer fractionated courses. In the spine, bowel can migrate close to tumors within vertebral bodies, requiring anatomic adaptation to avoid mobile bowel on a daily basis (108). Examples of the anatomic adaptive workflows of MRgRT are shown in **Figure 2**.

While these short courses give a limited amount of time for physiologic adaptation, studies have shown that mpMRI changes correlate with response to treatment as early as 1 day and 1 week after treatment for animal models (112) and brain metastasis patients (113), respectively. Therefore, daily monitoring with MRgRT may allow for plan adaptation even in such cases. Despite the short treatment time, radiomics analysis of imaging features on the 0.35T MRgRT system were shown to correlate with outcome in pancreatic cancer (114).

CONCLUSIONS

Novel MRgRT systems provide the first capability to perform high frequency mpMRI during conventional chemoradiotherapy of brain tumors and provide a platform for physiologic adaptive radiotherapy. The references in this manuscript suggest that combining different MRI modalities to trend tumor volume and relaxation (T1/T2/T2* mapping), metabolism (MRS), hypoxia (perfusion), and cellular density (DWI) may permit a better understanding of glioblastoma response to treatment and enable dose escalated radiotherapy to portions of tumor responding inappropriately to treatment in efforts to improve patient survival. The anatomic benefits of MRI may also permit anatomic adaptation in several scenarios such as stereotactic brain and spine tumor courses.

AUTHOR CONTRIBUTIONS

DM, MS, and EM contributed to the elaboration of the manuscript text and figures equally. All authors equally contributed on selecting literature and topics for revision and discussion, reviewing, and organizing the manuscript.

FUNDING

REFERENCES

1. Chin S, Eccles CL, McWilliam A, Chuter R, Walker E, Whitehurst P, et al. Magnetic resonance-guided radiation therapy: a review. *J Med Imaging Radiat Oncol.* (2020) 64:163–77. doi: 10.1111/1754-9485.12968

2. Mehta S, Gajjar SR, Padgett KR, Asher D, Stoyanova R, Ford JC, et al. Daily tracking of glioblastoma resection cavity, cerebral edema, and tumor volume with MRI-guided radiation therapy. *Cureus.* (2018) 10:e2346. doi: 10.7759/cureus.2346

3. Thomas DH, Santhanam A, Kishan AU, Cao M, Lamb J, Min Y, et al. Initial clinical observations of intra- and interfractional motion variation in MR-guided lung SBRT. *Br J Radiol.* (2018) 91:20170522. doi: 10.1259/bjr.20170522

4. Acharya S, Fischer-Valuck BW, Mazur TR, Curcuru A, Sona K, Kashani R, et al. Magnetic resonance image guided radiation therapy for external beam accelerated partial-breast irradiation: evaluation of delivered dose and intrafractional cavity motion. *Int J Radiat Oncol Biol Phys.* (2016) 96:785–92. doi: 10.1016/j.ijrobp.2016.08.006

5. Ramey SJ, Padgett KR, Lamichhane N, Neboori HJ, Kwon D, Mellon EA, et al. Dosimetric analysis of stereotactic body radiation therapy for pancreatic cancer using MR-guided Tri-(60)Co unit, MR-guided LINAC, and conventional LINAC-based plans. *Pract Radiat Oncol.* (2018) 8:e312–21. doi: 10.1016/j.prro.2018.02.010

6. Rudra S, Jiang N, Rosenberg SA, Olsen JR, Roach MC, Wan L, et al. Using adaptive magnetic resonance image-guided radiation therapy for treatment of inoperable pancreatic cancer. *Cancer Med.* (2019) 8:2123–32. doi: 10.1002/cam4.2100

7. Henke L, Kashani R, Robinson C, Curcuru A, DeWees T, Bradley J, et al. Phase I trial of stereotactic MR-guided online adaptive radiation therapy (SMART) for the treatment of oligometastatic or unresectable primary malignancies of the abdomen. *Radiother Oncol.* (2018) 126:519–26. doi: 10.1016/j.radonc.2017.11.032

8. Tetar Shyama U, Bruynzeel Anna ME, Lagerwaard Frank J, Slotman Ben J, Omar B, Palacios Miguel A. Clinical implementation of magnetic resonance imaging guided adaptive radiotherapy for localized prostate cancer. *Phys Imaging Radiat Oncol.* (2019) 9:69–76. doi: 10.1016/j.phro.2019.02.002

9. Asher D, Padgett KR, Llorente RE, Farnia BS, Ford JC, Gajjar SR, et al. Magnetic resonance-guided external beam radiation and brachytherapy for a patient with intact cervical cancer. *Cureus.* (2018) 10:e2577. doi: 10.7759/cureus.2577

10. van Sörnsen de. Koste JR, Palacios MA, Bruynzeel AME, Slotman BJ, Senan S, Lagerwaard FJ. MR-guided gated stereotactic radiation therapy delivery for lung, adrenal, and pancreatic tumors: a geometric analysis. *Int J Radiat Oncol Biol Phys.* (2018) 102:858–66. doi: 10.1016/j.ijrobp.2018.05.048

11. Simonetto C, Eidemüller M, Gaasch A, Pazos M, Schönecker S, Reitz D, et al. Does deep inspiration breath-hold prolong life? Individual risk estimates of ischaemic heart disease after breast cancer radiotherapy. *Radiother Oncol.* (2019) 131:202–07. doi: 10.1016/j.radonc.2018.07.024

12. El-Bared N, Portelance L, Spieler BO, Kwon D, Padgett KR, Brown KM, et al. Dosimetric benefits and practical pitfalls of daily online adaptive mri-guided stereotactic radiation therapy for pancreatic cancer. *Pract Radiat Oncol.* (2019) 9:e46–54. doi: 10.1016/j.prro.2018.08.010

13. Schmid RK, Tai A, Klawikowski S, Straza M, Ramahi K, Li XA, et al. The dosimetric impact of interfractional organ-at-risk movement during liver stereotactic body radiation therapy. *Pract Radiat Oncol.* (2019) 9:e549–58. doi: 10.1016/j.prro.2019.05.014

14. Ellingson BM, Malkin MG, Rand SD, Connelly JM, Quinsey C, LaViolette PS, et al. Validation of functional diffusion maps (fDMs) as a biomarker for human glioma cellularity. *J Magn Reson Imaging.* (2010) 31:538–48. doi: 10.1002/jmri.22068

15. Hein Patrick A, Eskey Clifford J, Dunn Jeffrey F, Hug Eugen B. Diffusion-weighted imaging in the follow-up of treated high-grade gliomas: tumor recurrence versus radiation injury. *AJNR.* (2004) 25:201–9.

16. Larsson C, Groote I, Vardal J, Kleppestø M, Odland A, Brandal P, et al. Prediction of survival and progression in glioblastoma patients using temporal perfusion changes during radiochemotherapy. *Magn Reson Imaging.* (2020) 68:106–12. doi: 10.1016/j.mri.2020.01.012

17. Pirzkall A, McKnight TR, Graves EE, Carol MP, Sneed PK, Wara WW, et al. MR-spectroscopy guided target delineation for high-grade gliomas. *Int J Radiat Oncol Biol Phys.* (2001) 50:915–28. doi: 10.1016/S0360-3016(01)01548-6

18. Hamstra DA, Rehemtulla A, Ross BD. Diffusion magnetic resonance imaging: a biomarker for treatment response in oncology. *J Clin Oncol.* (2007) 25:4104–9. doi: 10.1200/JCO.2007.11.9610

19. Mangla R, Singh G, Ziegelitz D, Milano MT, Korones DN, Zhong J, et al. Changes in relative cerebral blood volume 1 month after radiation-temozolomide therapy can help predict overall survival in patients with glioblastoma. *Radiology.* (2010) 256:575–84. doi: 10.1148/radiol.10091440

20. Muruganandham M, Clerkin PP, Smith BJ, Anderson CM, Morris A, Capizzano AA, et al. 3-Dimensional magnetic resonance spectroscopic imaging at 3 Tesla for early response assessment of glioblastoma patients during external beam radiation therapy. *Int J Radiat Oncol Biol Phys.* (2014) 90:181–9. doi: 10.1016/j.ijrobp.2014.05.014

21. Kupelian P, Sonke JJ. Magnetic resonance-guided adaptive radiotherapy: a solution to the future. *Semin Radiat Oncol.* (2014) 24:227–32. doi: 10.1016/j.semradonc.2014.02.013

22. Winkfield KM, Linsenmeier C, Yock TI, Grant PE, Yeap BY, Butler WE, et al. Surveillance of craniopharyngioma cyst growth in children treated with proton radiotherapy. *Int J Radiat Oncol Biol Phys.* (2009) 73:716–21. doi: 10.1016/j.ijrobp.2008.05.010

23. Stupp R, Taillibert S, Kanner A, Read W, Steinberg D, Lhermitte B, et al. Effect of tumor-treating fields plus maintenance temozolomide vs maintenance temozolomide alone on survival in patients with glioblastoma: a randomized clinical trial. *JAMA.* (2017) 318:2306–16. doi: 10.1001/jama.2017.18718

24. Li J, Wang M, Won M, Shaw EG, Coughlin C, Curran WJ Jr, et al. Validation and simplification of the radiation therapy oncology group recursive partitioning analysis classification for glioblastoma. *Int J Radiat Oncol Biol Phys.* (2011) 81:623–30. doi: 10.1016/j.ijrobp.2010.06.012

25. Ostrom QT, Cioffi G, Gittleman H, Patil N, Waite K, Kruchko C, et al. CBTRUS statistical report: primary brain and other central nervous system tumors diagnosed in the United States in 2012-2016. *Neuro Oncol.* (2019) 21:v1–100. doi: 10.1093/neuonc/noz150

26. Stupp R, Mason WP, van den Bent MJ, Weller M, Fisher B, Taphoorn MJ, et al. Radiotherapy plus concomitant and adjuvant temozolomide for glioblastoma. *N Engl J Med.* (2005) 352:987–96. doi: 10.1056/NEJMoa043330

27. Wen PY, Macdonald DR, Reardon DA, Cloughesy TF, Sorensen AG, Galanis E, et al. Updated response assessment criteria for high-grade gliomas: response assessment in neuro-oncology working group. *J Clin Oncol.* (2010) 28:1963–72. doi: 10.1200/JCO.2009.26.3541

28. Brandes AA, Franceschi E, Tosoni A, Blatt V, Pession A, Tallini G, et al. MGMT promoter methylation status can predict the incidence and outcome of pseudoprogression after concomitant radiochemotherapy in newly diagnosed glioblastoma patients. *J Clin Oncology.* (2008) 26:2192–7. doi: 10.1200/JCO.2007.14.8163

29. Taal W, Brandsma D, de Bruin HG, Bromberg JE, Swaak-Kragten AT, Smitt PA, et al. Incidence of early pseudo-progression in a cohort of malignant

glioma patients treated with chemoirradiation with temozolomide. *Cancer.* (2008) 113:405–10. doi: 10.1002/cncr.23562

30. Brandes AA, Tosoni A, Spagnolli F, Frezza G, Leonardi M, Calbucci F, et al. Disease progression or pseudoprogression after concomitant radiochemotherapy treatment: pitfalls in neurooncology. *Neuro Oncol.* (2008) 10:361–7. doi: 10.1215/15228517-2008-008

31. Chaskis C, Neyns B, Michotte A, De Ridder M, Everaert H. Pseudoprogression after radiotherapy with concurrent temozolomide for high-grade glioma: clinical observations and working recommendations. *Surg Neurol.* (2009) 72:423–8. doi: 10.1016/j.surneu.2008.09.023

32. Fabi A, Russillo M, Metro G, Vidiri A, Di Giovanni S, Cognetti F. Pseudoprogression and MGMT status in glioblastoma patients: implications in clinical practice. *Anticancer Res.* (2009) 29:2607–10.

33. Young RJ, Gupta A, Shah AD, Graber JJ, Zhang Z, Shi W, et al. Potential utility of conventional MRI signs in diagnosing pseudoprogression in glioblastoma. *Neurology.* (2011) 76:1918–24. doi: 10.1212/WNL.0b013e31821d74e7

34. Jones KK, Dooley S, Maziero D, Ford JC, Stoyanova R, Goryawala M, et al. MRI-guided radiotherapy identifies early pseudoprogression of glioblastoma. *Research Square [Preprint].* (2020) doi: 10.21203/rs.3.rs-42434/v1

35. Stewart J, Sahgal A, Lee Y, Soliman H, Tseng C-L, Detsky J, et al. Quantitating interfraction target dynamics during concurrent chemoradiation for glioblastoma: a prospective serial imaging study. *Int J Radiat Oncol Biol Phys.* (2021) 109:736–46. doi: 10.1016/j.ijrobp.2020.10.002

36. Garcia J, Liu SZ, Louie AY. Biological effects of MRI contrast agents: gadolinium retention, potential mechanisms and a role for phosphorus. *Philos Trans A Math Phys Eng Sci.* (2017) 375:180. doi: 10.1098/rsta.2017.0180

37. Reddy K, Westerly D, Chen C. MRI patterns of T1 enhancing radiation necrosis versus tumour recurrence in high-grade gliomas. *J Med Imaging Radiat Oncol.* (2013) 57:349–55. doi: 10.1111/j.1754-9485.2012. 02472.x

38. Booth TC, Larkin TJ, Yuan Y, Kettunen MI, Dawson SN, Scoffings D, et al. Analysis of heterogeneity in T2-weighted MR images can differentiate pseudoprogression from progression in glioblastoma. *PLoS ONE.* (2017) 12:e0176528. doi: 10.1371/journal.pone.0176528

39. Sugahara T, Korogi Y, Kochi M, Ikushima I, Hirai T, Okuda T, et al. Correlation of MR imaging-determined cerebral blood volume maps with histologic and angiographic determination of vascularity of gliomas. *AJR Am J oentgenol.* (1998) 171:1479–86. doi: 10.2214/ajr.171.6.9843274

40. Reimer C, Deike K, Graf M, Reimer P, Wiestler B, Floca RO, et al. Differentiation of pseudoprogression and real progression in glioblastoma using ADC parametric response maps. *PLoS ONE.* (2017) 12:e0174620. doi: 10.1371/journal.pone.0174620

41. Crawford FW, Khayal IS, McGue C, Saraswathy S, Pirzkall A, Cha S, et al. Relationship of pre-surgery metabolic and physiological MR imaging parameters to survival for patients with untreated GBM. *J Neurooncol.* (2009) 91:337–51. doi: 10.1007/s11060-008-9719-x

42. Weiskopf N, Suckling J, Williams G, Correia M, Inkster B, Tait R, et al. Quantitative multi-parameter mapping of R1, PD*, MT, and R2* at 3T: a multi-center validation. *Front Neurosci.* (2013) 7:95. doi: 10.3389/fnins.2013.00095

43. Blystad I, Warntjes JB, Marcel SÖ, Lundberg P, Larsson E-M, Tisell A. Quantitative MRI for analysis of peritumoral edema in malignant gliomas. *PLoS ONE.* (2017) 12:e0177135. doi: 10.1371/journal.pone.0177135

44. Hattingen E, Müller A, Jurcoane A, Mädler B, Ditter P, Schild H, et al. Value of quantitative magnetic resonance imaging T1-relaxometry in predicting contrast-enhancement in glioblastoma patients. *Oncotarget.* (2017) 8:53542–51. doi: 10.18632/oncotarget.18612

45. Lescher S, Jurcoane A, Veit A, Bähr O, Deichmann R, Hattingen E. Quantitative T1 and T2 mapping in recurrent glioblastomas under bevacizumab: earlier detection of tumor progression compared to conventional MRI. *Neuroradiology.* (2015) 57:11–20. doi: 10.1007/s00234-014-1445-9

46. Chen Y, Liu S, Wang Y, Kang Y, Haacke EM. Strategically acquired gradient echo (STAGE) imaging, part I: creating enhanced T1 contrast and standardized susceptibility weighted imaging and quantitative susceptibility mapping. *Magn Reson Imaging.* (2018) 46:130–9. doi: 10.1016/j.mri.2017.10.005

47. Nejad-Davarani SP, Zakariaei N, Chen Y, Haacke E, Mark H Jr, Newton J, et al. Rapid multicontrast brain imaging on a 0.35T MR-linac. *Med Phys.* (2020) 47:4064–76. doi: 10.1002/mp.14251

48. Bruijnen T, van der Heide O, Intven MPW, Mook S, Lagendijk JJW, van den Berg CAT, et al. Technical feasibility of magnetic resonance fingerprinting on a 1.5 T MRI-Linac. *Phys Med Biol.* (2020) 65:22NT01. doi: 10.1088/1361-6560/abbb9d

49. Belliveau JW, Rosen BR, Kantor HL, Rzedzian RR, Kennedy DN, McKinstry RC, et al. Functional cerebral imaging by susceptibility-contrast NMR. *Magn Reson Med.* (1990) 14:538–46. doi: 10.1002/mrm.1910140311

50. Paldino MJ, Barboriak DP. Fundamentals of quantitative dynamic contrast-enhanced MR imaging. *Magn Reson Imaging Clin N Am.* (2009) 17:277–89. doi: 10.1016/j.mric.2009.01.007

51. Petrella JR, Provenzale JM. MR perfusion imaging of the brain. *Am J Roentgenol.* (2000) 175:207–19. doi: 10.2214/ajr.175.1.1750207

52. Østergaard L. Principles of cerebral perfusion imaging by bolus tracking. *J Magn Reson Imaging.* (2005) 22:710–7. doi: 10.1002/jmri.20460

53. Welker K, Boxerman J, Kalnin A, Kaufmann T, Shiroishi M, Wintermark M. ASFNR recommendations for clinical performance of MR dynamic susceptibility contrast perfusion imaging of the brain. *AJNR.* (2015) 36:E41–51. doi: 10.3174/ajnr.A4341

54. Patel P, Baradaran H, Delgado D, Askin G, Christos P, John Tsiouris A, et al. MR perfusion-weighted imaging in the evaluation of high-grade gliomas after treatment: a systematic review and meta-analysis. *Neuro Oncol.* (2017) 19:118–27. doi: 10.1093/neuonc/now148

55. Hu LS, Baxter LC, Smith KA, Feuerstein BG, Karis JP, Eschbacher JM, et al. Relative cerebral blood volume values to differentiate high-grade glioma recurrence from posttreatment radiation effect: direct correlation between image-guided tissue histopathology and localized dynamic susceptibility-weighted contrast-enhanced perfusion MR imaging measurements. *AJNR.* (2009) 30:552–8. doi: 10.3174/ajnr.A1377

56. Barajas RF Jr, Chang JS, Segal MR, Parsa AT, McDermott MW, Berger MS, et al. Differentiation of recurrent glioblastoma multiforme from radiation necrosis after external beam radiation therapy with dynamic susceptibility-weighted contrast-enhanced perfusion MR imaging. *Radiology.* (2009) 253:486–96. doi: 10.1148/radiol.2532090007

57. Yankeelov TE, Gore JC. Dynamic contrast enhanced magnetic resonance imaging in oncology: theory, data acquisition, analysis, and examples. *Curr Med Imaging Rev.* (2009) 3:91–107. doi: 10.2174/157340507780619179

58. O'Connor JP, Tofts PS, Miles KA, Parkes LM, Thompson G, Jackson A. Dynamic contrast-enhanced imaging techniques: CT and MRI. *Br J Radiol.* (2011) 84:S112–20. doi: 10.1259/bjr/55166688

59. Bisdas S, Naegele T, Ritz R, Dimostheni A, Pfannenberg C, Reimold M, et al. Distinguishing recurrent high-grade gliomas from radiation injury: a pilot study using dynamic contrast-enhanced MR imaging. *Acad Radiol.* (2011) 18:575–83. doi: 10.1016/j.acra.2011.01.018

60. Thomas AA, Arevalo-Perez J, Kaley T, Lyo J, Peck KK, Shi W, et al. Dynamic contrast enhanced T1 MRI perfusion differentiates pseudoprogression from recurrent glioblastoma. *J Neurooncol.* (2015) 125:183–90. doi: 10.1007/s11060-015-1893-z

61. Yun TJ, Park CK, Kim TM, Lee SH, Kim JH, Sohn CH, et al. Glioblastoma treated with concurrent radiation therapy and temozolomide chemotherapy: differentiation of true progression from pseudoprogression with quantitative dynamic contrast-enhanced MR imaging. *Radiology.* (2015) 274:830–40. doi: 10.1148/radiol.14132632

62. Møller S, Lundemann M, Law I, Poulsen HS, Larsson HBW, Engelholm SA. Early changes in perfusion of glioblastoma during radio- and chemotherapy evaluated by T1-dynamic contrast enhanced magnetic resonance imaging. *Acta Oncologica.* (2015) 54:1521–8. doi: 10.3109/0284186X.2015.1063777

63. Galban CJ, Chenevert TL, Meyer CR, Tsien C, Lawrence TS, Hamstra DA, et al. The parametric response map is an imaging biomarker for early cancer treatment outcome. *Nat Med.* (2009) 15:572–6. doi: 10.1038/nm.1919

64. Tsien C, Galbán CJ, Chenevert TL, Johnson TD, Hamstra DA, Sundgren PC, et al. Parametric response map as an imaging biomarker to distinguish progression from pseudoprogression in high-grade glioma. *J Clin Oncol.* (2010) 28:2293–9. doi: 10.1200/JCO.2009.25.3971

65. Batchelor TT, Gerstner ER, Emblem KE, Duda DG, Kalpathy-Cramer J, Snuderl M, et al. Improved tumor oxygenation and survival in glioblastoma patients who show increased blood perfusion after cediranib and chemoradiation. *Proc Natl Acad Sci USA*. (2013) 110:19059–64. doi: 10.1073/pnas.1318022110

66. Williams DS, Detre JA, Leigh JS, Koretsky AP. Magnetic resonance imaging of perfusion using spin inversion of arterial water. *Proc Natl Acad Sci USA*. (1992) 89:212–6. doi: 10.1073/pnas.89.1.212

67. Le Bihan D, Breton E, Lallemand D, Grenier P, Cabanis E, Laval-Jeantet M. MR imaging of intravoxel incoherent motions: application to diffusion and perfusion in neurologic disorders. *Radiology*. (1986) 161:401–7. doi: 10.1148/radiology.161.2.3763909

68. Federau C, Cerny M, Roux M, Mosimann PJ, Maeder P, Meuli R, et al. IVIM perfusion fraction is prognostic for survival in brain glioma. *Clin Neuroradiol*. (2017) 27:485–92. doi: 10.1007/s00062-016-0510-7

69. Choi YJ, Kim HS, Jahng GH, Kim SJ, Suh DC. Pseudoprogression in patients with glioblastoma: added value of arterial spin labeling to dynamic susceptibility contrast perfusion MR imaging. *Acta Radiol*. (2013) 54:448–54. doi: 10.1177/0284185112474916

70. Mori S, Barker PB. Diffusion magnetic resonance imaging: its principle and applications. *Anat Rec*. (1999) 257:102–9. doi: 10.1002/(SICI)1097-0185(19990615)257:3<102::AID-AR7>3.0.CO;2-6

71. Nakamura H, Murakami R, Hirai T, Kitajima M, Yamashita Y. Can MRI-derived factors predict the survival in glioblastoma patients treated with postoperative chemoradiation therapy? *Acta Radiol*. (2013) 54:214–20. doi: 10.1258/ar.2012.120525

72. Saraswathy S, Crawford FW, Lamborn KR, Pirzkall A, Chang S, Cha S, et al. Evaluation of MR markers that predict survival in patients with newly diagnosed GBM prior to adjuvant therapy. *J Neurooncol*. (2009) 91:69–81. doi: 10.1007/s11060-008-9685-3

73. Chang PD, Chow DS, Yang PH, Filippi CG, Lignelli A. Predicting glioblastoma recurrence by early changes in the apparent diffusion coefficient value and signal intensity on FLAIR images. *Am J Roentgenol*. (2016) 208:57–65. doi: 10.2214/AJR.16.16234

74. Wang S, Martinez-Lage M, Sakai Y, Chawla S, Kim SG, Alonso-Basanta M, et al. Differentiating tumor progression from pseudoprogression in patients with glioblastomas using diffusion tensor imaging and dynamic susceptibility contrast MRI. *AJNR Am J Neuroradiol*. (2016) 37:28–36. doi: 10.3174/ajnr.A4474

75. Elson A, Bovi J, Siker M, Schultz C, Paulson E. Evaluation of absolute and normalized apparent diffusion coefficient (ADC) values within the post-operative T2/FLAIR volume as adverse prognostic indicators in glioblastoma. *J Neuro Oncol*. (2015) 122:549–58. doi: 10.1007/s11060-015-1743-z

76. Moffat BA, Chenevert TL, Lawrence TS, Meyer CR, Johnson TD, Dong Q, et al. Functional diffusion map: a noninvasive MRI biomarker for early stratification of clinical brain tumor response. *Proc Natl Acad Sci USA*. (2005) 102:5524–9. doi: 10.1073/pnas.0501532102

77. Hamstra DA, Chenevert TL, Moffat BA, Johnson TD, Meyer CR, Mukherji SK, et al. Evaluation of the functional diffusion map as an early biomarker of time-to-progression and overall survival in high-grade glioma. *Proc Natl Acad Sci USA*. (2005) 102:16759–64. doi: 10.1073/pnas.0508347102

78. Moffat BA, Chenevert TL, Meyer CR, McKeever PE, Hall DE, Hoff BA, et al. The functional diffusion map: an imaging biomarker for the early prediction of cancer treatment outcome. *Neoplasia*. (2006) 8:259–67. doi: 10.1593/neo.05844

79. Hamstra DA, Galban CJ, Meyer CR, Johnson TD, Sundgren PC, Tsien C, et al. Functional diffusion map as an early imaging biomarker for high-grade glioma: correlation with conventional radiologic response and overall survival. *J Clin Oncol*. (2008) 26:3387–94. doi: 10.1200/JCO.2007.15.2363

80. Chenevert TL, Malyarenko DI, Galbán CJ, Gomez-Hassan DM, Sundgren PC, Tsien CI, et al. Comparison of voxel-wise and histogram analyses of glioma ADC maps for prediction of early therapeutic change. *Tomography*. (2019) 5:7–14. doi: 10.18383/j.tom.2018.00049

81. Yang Y, Cao M, Sheng K, Gao Y, Chen A, Kamrava M, et al. Longitudinal diffusion MRI for treatment response assessment: preliminary experience using an MRI-guided tri-cobalt 60 radiotherapy system. *Med Phys*. (2016) 43:1369–73. doi: 10.1118/1.4942381

82. Ott D, Hennig J, Ernst T. Human brain tumors: assessment with *in vivo* proton MR spectroscopy. *Radiology*. (1993) 186:745–52. doi: 10.1148/radiology.186.3.8430183

83. Croteau D, Scarpace L, Hearshen D, Gutierrez J, Fisher JL, Rock JP, et al. Correlation between magnetic resonance spectroscopy imaging and image-guided biopsies: semiquantitative and qualitative histopathological analyses of patients with untreated glioma. *Neurosurgery*. (2001) 49:823–9. doi: 10.1227/00006123-200110000-00008

84. Shimizu H, Kumabe T, Shirane R, Yoshimoto T. Correlation between choline level measured by proton MR spectroscopy and Ki-67 labeling index in Gliomas. *AJNR*. (2000) 21:659–65.

85. Herminghaus S, Pilatus U, Möller-Hartmann W, Raab P, Lanfermann H, Schlote W, et al. Increased choline levels coincide with enhanced proliferative activity of human neuroepithelial brain tumors. *NMR Biomed*. (2002) 15:385–92. doi: 10.1002/nbm.793

86. Di Costanzo A, Scarabino T, Trojsi F, Giannatempo GM, Popolizio T, Catapano D, et al. Multiparametric 3T MR approach to the assessment of cerebral gliomas: tumor extent and malignancy. *Neuroradiology*. (2006) 48:622–31. doi: 10.1007/s00234-006-0102-3

87. Di Costanzo A, Trojsi F, Giannatempo GM, Vuolo L, Popolizio T, Catapano D, et al. Spectroscopic, diffusion and perfusion magnetic resonance imaging at 3.0 Tesla in the delineation of glioblastomas: preliminary results. *J Exp Clin Cancer Res*. (2006) 25:383–90.

88. Cordova JS, Shu HK, Liang Z, Gurbani SS, Cooper LA, Holder CA, et al. Whole-brain spectroscopic MRI biomarkers identify infiltrating margins in glioblastoma patients. *Neuro Oncol*. (2016) 18:1180–9. doi: 10.1093/neuonc/now036

89. Parra N, Andres MAA, Gupta RK, Ishkanian F, Huang K, Walker GR, et al. Volumetric spectroscopic imaging of glioblastoma multiforme radiation treatment volumes. *Int J Radiat Oncol Biol Phys*. (2014) 90:376–84. doi: 10.1016/j.ijrobp.2014.03.049

90. Mellon E, Gurbani S, Ramesh K, Weinberg B, Kleinberg L, Schreibmann E, et al. ACTR-70. A multisite clinical trial of spectroscopic MRI-guided radiation dose escalation in glioblastoma patients. *Neuro Oncol*. (2019) 21:vi29–30. doi: 10.1093/neuonc/noz175.111

91. Quon H, Brunet B, Alexander A, Murtha A, Abdulkarim B, Fulton D, et al. Changes in serial magnetic resonance spectroscopy predict outcome in high-grade glioma during and after postoperative radiotherapy. *Anticancer Res*. (2011) 31:3559–65. doi: 10.3969/j.issn.1673-5374.2013.29.009

92. Natarajan SK, Venneti S. Glutamine metabolism in brain tumors. *Cancers*. (2019) 11. doi: 10.3390/cancers11111628

93. Prost Robert W, Mark L, Mewissen M, Li S-J. Detection of glutamate/glutamine resonances by 1H magnetic resonance spectroscopy at 0.5 tesla. *Magn Reson Med*. (1997) 37:615–18. doi: 10.1002/mrm.1910370422

94. Gurbani S, Weinberg B, Cooper L, Mellon E, Schreibmann E, Sheriff S, et al. The brain imaging collaboration suite (BrICS): a cloud platform for integrating whole-brain spectroscopic MRI into the radiation therapy planning workflow. *Tomography*. (2019) 5:184–91. doi: 10.18383/j.tom.2018.00028

95. Ramesh K, Gurbani SS, Mellon EA, Huang V, Goryawala M, Barker PB, et al. The longitudinal imaging tracker (BrICS-LIT): a cloud platform for monitoring treatment response in glioblastoma patients. *Tomography*. (2020) 6:93–100. doi: 10.18383/j.tom.2020.00001

96. Aerts Hugo JWL, Velazquez ER, Leijenaar RTH, Parmar C, Grossmann P, Carvalho S, et al. Decoding tumour phenotype by noninvasive imaging using a quantitative radiomics approach'. *Nat Commun*. (2014) 5:4006. doi: 10.1038/ncomms5644

97. McGarry SD, Hurrell SL, Kaczmarowski AL, Cochran EJ, Connelly J, Rand SD, et al. Magnetic resonance imaging-based radiomic profiles predict patient prognosis in newly diagnosed glioblastoma before therapy. *Tomography*. (2016) 2:223–8. doi: 10.18383/j.tom.2016.00250

98. Park JE, Kim HS, Jo Y, Yoo R-E, Choi SH, Nam SJ, et al. Radiomics prognostication model in glioblastoma using diffusion- and perfusion-weighted MRI. *Sci Rep*. (2020) 10:4250. doi: 10.1038/s41598-020-61178-w

99. Rettenmeier C, Maziero D, Qian Y, Stenger VA. A circular echo planar sequence for fast volumetric fMRI. *Magn Reson Med.* (2019) 81:1685–98. doi: 10.1002/mrm.27522

100. Mehranian A, McGinnity CJ, Neji R, Prieto C, Hammers A, De Vita E, et al. Motion-corrected and high-resolution anatomically assisted (MOCHA) reconstruction of arterial spin labeling MRI. *Magn Reson Med.* (2020) 84:1306–20. doi: 10.1002/mrm.28205

101. Lin H, Figini M, Tanno R, Blumberg SB, Kaden E, Ogbole G, et al. Deep learning for low-field to high-field MR: image quality transfer with probabilistic decimation simulator. In: *International Workshop on Machine Learning for Medical Image Reconstruction.* Cham: Springer International Publishing (2019). p. 58–70.

102. Sun J, Guo M, Pang H, Qi J, Zhang J, Ge Y. Treatment of malignant glioma using hyperthermia. *Neural Regen Res.* (2013) 8:2775–82.

103. Cao-Pham T-T, Tran L-B-A, Colliez F, Joudiou N, El BS, Grégoire V, et al. Monitoring tumor response to carbogen breathing by oxygen-sensitive magnetic resonance parameters to predict the outcome of radiation therapy: a preclinical study. *Int J Radiat Oncol Biol Phys.* (2016) 96:149–60. doi: 10.1016/j.ijrobp.2016.04.029

104. Breto AL, Padgett KR, Ford JC, Kwon D, Chang C, Fuss M, et al. Analysis of magnetic resonance image signal fluctuations acquired during MR-guided radiotherapy. *Cureus.* (2018) 10:e2385. doi: 10.7759/cureus.2385

105. Llorente R, Spieler BO, Victoria J, Takita C, Yechieli R, Ford JC, et al. MRI-guided stereotactic ablative radiation therapy of spinal bone metastases: a preliminary experience. *Br J Radiol.* (2020) 93:20190655. doi: 10.1259/bjr.20190655

106. Atalar B, Choi CYH, Harsh GR, IV, Chang Steven D, Gibbs IC, Adler JR, et al. Cavity volume dynamics after resection of brain metastases and timing of postresection cavity stereotactic radiosurgery. *Neurosurgery.* (2012) 72:180–5. doi: 10.1227/NEU.0b013e31827b99f3

107. Salkeld Alison L, Hau Eric KC, Nahar N, Sykes JR, Wang W, Thwaites DI. Changes in brain metastasis during radiosurgical planning. *Int J Radiat Oncol Biol Phys.* (2018) 102:727–33. doi: 10.1016/j.ijrobp.2018.06.021

108. Spieler B, Samuels SE, Llorente R, Yechieli R, Ford JC, Mellon EA. Advantages of radiation therapy simulation with 0.35 tesla magnetic resonance imaging for stereotactic ablation of spinal metastases. *Pract Radiat Oncol.* (2020) 10:339–44. doi: 10.1016/j.prro.2019.10.018

109. Winkel D, Bol GH, Kroon PS, van Asselen B, Hackett SS, Werensteijn-Honingh AM, et al. Adaptive radiotherapy: the Elekta unity MR-linac concept. *Clin Transl Radiat Oncol.* (2019) 18:54–9. doi: 10.1016/j.ctro.2019.04.001

110. Hal WA, Straza MW, Chen X, Mickevicius N, Erickson B, Schultz C, et al. Initial clinical experience of stereotactic body radiation therapy (SBRT) for liver metastases, primary liver malignancy, and pancreatic cancer with 4D-MRI based online adaptation and real-time MRI monitoring using a 1.5 Tesla MR-Linac. *PLoS ONE.* (2020) 15:e0236570. doi: 10.1371/journal.pone.0236570

111. Paulson ES, Ahunbay E, Chen X, Mickevicius NJ, Chen GP, Schultz C, et al. 4D-MRI driven MR-guided online adaptive radiotherapy for abdominal stereotactic body radiation therapy on a high field MR-Linac: implementation and initial clinical experience. *Clin Transl Radiat Oncol.* (2020) 23:72–9. doi: 10.1016/j.ctro.2020.05.002

112. Zhou H, Zhang Z, Denney R, Williams JS, Gerberich J, Stojadinovic S, et al. Tumor physiological changes during hypofractionated stereotactic body radiation therapy assessed using multi-parametric magnetic resonance imaging. *Oncotarget.* (2017) 8:37464–77. doi: 10.18632/oncotarget.16395

113. Jakubovic R, Sahgal A, Soliman H, Milwid R, Zhang L, Eilaghi A, et al. Magnetic resonance imaging-based tumour perfusion parameters are biomarkers predicting response after radiation to brain metastases. *Clin Oncol.* (2014) 26:704–12. doi: 10.1016/j.clon.2014.06.010

114. Simpson G, Spieler B, Dogan N, Portelance L, Mellon EA, Kwon D, et al. Predictive value of 0.35 T magnetic resonance imaging radiomic features in stereotactic ablative body radiotherapy of pancreatic cancer: a pilot study. *Med Phys.* (2020) 47:3682–90. doi: 10.1002/mp.14200